134 RAPID-SCAN DUAL-POLARIZATION WSR-88D OBSERVATIONS OF AN OKLAHOMA HAILSTORM PRODUCING EXTREMELY-LARGE HAIL

ARTHUR WITT* AND DON W. BURGESS

NOAA/National Severe Storms Laboratory, Norman, OK

ANTON SEIMON

Appalachian State University, Boone, NC

JOHN T. ALLEN

IRI/Columbia University, Palisades, NY

1. INTRODUCTION

On 31 May 2013, an outbreak of severe thunderstorms occurred across central OK, resulting in one of the most extreme tornado and hail events recorded to date. Numerous hailstones from 10 cm to at least 16 cm in diameter were observed across a $\sim$50 km^2 domain on the west side of El Reno, OK from 2300–2330 UTC originating from the El Reno Storm, a large tornadic supercell (Bluestein et al. 2015). The extremely-large hailstones fell within 60 km of the KOUN WSR-88D located in Norman, OK. As KOUN is not part of the operational WSR-88D network, it is able to scan more limited volumes of space via traditional "sector scans" (unlike most WSR-88D radars that only scan a full 360°). This allowed for higher time-resolution (compared to typical WSR-88D volume-scan time intervals) dual-polarization radar observations of the supercell storm that produced the giant hailstones. The study presented here examined the KOUN observations of the El Reno Storm, focusing on two locations where giant hail fall was observed.

FIG. 1. Picture of the 16 cm hailstone (photo from C. Parker).

2. GIANT HAILSTONE OBSERVATIONS

The observations of giant hail were obtained via social media sources (Hyvärinen and Saltikoff 2010) and the El Reno Survey Project (Seimon et al. 2014). Two extremely-large hailstones, approximately 13 cm to 16 cm in diameter, were observed in close proximity on the west side of El Reno. The 16 cm hailstone (Fig. 1) was reported on the KFOR-TV web page (photo #25 in the gallery at http://kfor.com/2013/06/04/update-el-reno-union-city-tornado-widest-tornado-on-record/). It fell at the home of C. Parker (926 S. Magnolia Street; latitude 35.5227°, longitude −97.9755°), located 304° and 56 km from KOUN. The 13 cm hailstone (Fig. 2) fell nearby (at 1817 Handley Drive; latitude 35.5243°, longitude −97.9777°), and was reported at https://www.reddit.com/r/Images/related/1ffyio/hail_in_el_reno_oklahoma_today/. Although the source and location of these two hail reports are known, as is often the case with observations obtained from social media, no time was mentioned as to when the hailstones actually fell. However, it was possible to obtain a reasonably accurate estimate of $\sim$2305 UTC as the time

*Corresponding author address: Arthur Witt, NOAA/National Severe Storms Laboratory, 120 David L. Boren Blvd., Norman, OK, 73072.

E-mail: Arthur.Witt@noaa.gov

FIG. 2. Picture of the 13 cm hailstone (photo from A. Stevens).

FIG. 3. Image of hailstones estimated to be ∼15 cm in diameter (from video provided by H. Farrar).

that these hailstones fell, based on images of giant hailstones seen falling between 2304 UTC and 2308 UTC in two videos taken at nearby locations (within 1 km). Additional confirmation comes from the dual-polarization radar data examined in this study, and a previous analysis of phased array radar observations of this storm (Witt 2014). At 2305 UTC, this location was in the storm's forward-flank region, northeast of the main updraft (Fig. 4), and hereafter will be referred to as the forward-flank hailfall (FFH).

A second location where giant hail was observed occurred southwest of the FFH location, on Jensen Road at latitude 35.4935°, longitude −98.0053°. The hailstones were observed at ∼2320 UTC in video recorded by H. Farrar (who kindly provided a copy of the video to the El Reno Survey Project) (Fig. 3). Based on a road width of 9 m, the hailstones are estimated to be ∼15 cm in diameter. At 2320 UTC, this location was in the storm's hook-echo region, west of the main updraft (Fig. 7), and hereafter will be referred to as the hook-echo hailfall (HEH).

3. KOUN SCANNING STRATEGY

For the time period analyzed in this study, KOUN scanned the El Reno Storm using the following strategy
Sector width: 90°–105°
Elevation angles (10): 0.52°, 0.97°, 1.5°, 2.05°, 3.05°, 4.05°, 5.05°, 5.95°, 7.97°, 9.9°
Update time: 98–100 s
Azimuthal sampling: 0.5°
Radial resolution: 250 m
Maximum range: 124 km
Nyquist velocity: 33.2 m s^{-1}

To allow for update times on the order of 1.5 min, the highest elevation angle used was 9.9°. Hence, the upper parts of the storm were not scanned (Fig. 4).

4. RADAR OBSERVATIONS

The evolution of the KOUN data above the FFH and HEH were examined as the storm passed over these locations. This included analysis of the variations in low-altitude reflectivity (LA-Z), differential reflectivity (LA-Z_{DR}), co-polar correlation coefficient (LA-ρ_{HV}) and specific differential phase (LA-K_{DP}) (see Kumjian 2013, for a description of the polarimetric radar variables). Measures of these variables on the lowest three elevation scans were calculated using the median value of the eight radar bins within a 1° x 1 km window centered on the location of the FFH and HEH. Also examined were vertical and horizontal cross-sections of these radar fields several minutes before and after the FFH and HEH. The vertical cross-sections were along the radar radial passing through the location of the FFH and HEH, with the horizontal cross-sections at 5 km above radar level (ARL).

a. Forward-Flank Hailfall

As the forward flank of the storm progressed over the FFH location, the LA-Z increased from ∼30 dBZ at 2228 UTC to a first relative maximum ∼50 dBZ at 2300 UTC (Fig. 8). The LA-Z then decreased to a relative minimum ∼41 dBZ at 2303 UTC, before increasing to maximum ∼55 dBZ at 2329 UTC, as the southern part of the storm's precipitation core passed over the FFH location. Similarly, the LA-Z_{DR} generally increased from ∼2.5 dB at 2228

UTC to a maximum ∼5 dB at 2301 UTC (Fig. 9), as the Z_{DR} shield (Romine et al. 2008) progressed over the FFH location. Then, the LA-Z_{DR} rapidly decreased, to a minimum ∼1 dB from 2305–2308 UTC, as the hail core associated with the FFH fell to the surface. Following this minimum, the LA-Z_{DR} increased to a relative maximum ∼4 dB from 2313–2317 UTC. As the storm's core passed over from 2318–2332 UTC, the LA-Z_{DR} cycled rapidly in magnitude, possibly due to variations in hailfall intensity (i.e., more hail was likely falling during periods of lower LA-Z_{DR}). Unlike the trend seen for LA-Z and LA-Z_{DR}, the LA-ρ_{HV} displayed a general decrease in magnitude from ∼1.0 at 2228 UTC to a minimum ∼0.92 at ∼2305 UTC (Fig. 10), after which it generally increased to ∼0.97 from 2323–2332 UTC, as the storm's core passed over. The LA-K_{DP} was relatively steady from 2228 UTC to 2301 UTC, generally ∼ 0–1° km^{-1} in magnitude (Fig. 11), after which it decreased to a minimum ∼ −1.0° km^{-1} at ∼2304 UTC. The LA-K_{DP} then increased to a maximum ∼2.5° km^{-1} at 2325 UTC, as the storm core passed over. Validation of the low LA-K_{DP} values observed from 2301–2309 UTC can be made based on little to no rainfall seen in video taken in the vicinity of the FFH, while at the same time, occasional giant hailstones were observed.

The descent of the hail core associated with the FFH is evident in the vertical cross sections of reflectivity, differential reflectivity and co-polar correlation coefficient (Figs. 4, 5, 6). As higher reflectivity (>50 dBZ) above the FFH location descends toward the surface from 2302–2306 UTC, there is a corresponding decrease in differential reflectivity (to <2 dB) and co-polar correlation coefficient (to <0.95).

b. Hook-Echo Hailfall

The HEH occurred within a relatively narrow arc of hail evident via a band of lower LA-Z_{DR} and LA-ρ_{HV} in the storm's hook echo (Fig. 7). The passage of this arc over the HEH location at ∼2320 UTC is most discernible in the time series of LA-ρ_{HV} (Fig. 14), seen by the rapid decrease from 0.98 at 2318 UTC to <0.9 at 2320 UTC, followed by a sharp increase back up to 0.98 after 2324 UTC. The LA-Z_{DR} showed a similar large decrease in magnitude, from >4.5 dB at ∼2316 UTC to a minimum ∼2 dB at ∼2321 UTC (Fig. 13), after which it remained ∼2 dB. Little variation was found in the time series of LA-K_{DP} (Fig. 15), although a relative minimum on the lowest two elevation angles did occurr from 2321–2323 UTC, somewhat later than the minimums seen in the time series of LA-ρ_{HV} and LA-Z_{DR}. Also noteworthy is the time series of LA-Z over the HEH location, in that the LA-Z never exceeded 45 dBZ (Fig. 12).

5. CONCLUSIONS

The damage potential and threat to life and property associated with a severe storm increases at a nonlinear rate as the intensity of the storm increases. Hence, timely identification and warning on the occurrence of extreme severe-weather events, such as very large damaging hail, is vital. The occurrence of near record-size hail, from 13–16 cm in diameter, within 60 km of the KOUN WSR-88D, provides the opportunity to examine the character and evolution of the storm that produced such as huge hailstones in greater detail than would be possible from operational radars scanning at slower rates.

For the two specific instances of giant hail examined in this study, some noteworthy findings are that the giant hailstones:

1) fell outside of the main precipitation core, in areas of the storm with LA-Z ≤45 dBZ;

2) were associated with dual-polarization radar signatures consistent with past observations of giant hail, namely relatively low Z_{DR}, ρ_{HV} and K_{DP} (Picca and Ryzhkov 2012; Smyth et al. 1999);

3) occurred along both the forward and back edges of the storm's main updraft;

4) were near a large tornado associated with a deep, intense mesocyclone.

Another important finding relates to the rapid evolution of the dual-polarization hail signatures seen in this case, which demonstrates the benefits of higher time-resolution radar observations. When radar variables that are associated with giant hail exhibit large changes in magnitude over time periods of 1–2 min, data update times on a similar scale will be necessary to observe these events. Also worth noting is that extreme severe-weather events have become better documented thanks to social media sources and efforts such as the El Reno Survey Project (Blair and Leighton 2012).

References

Blair, S. F., and J. W. Leighton, 2012: Creating high-resolution hail datasets using social media and post-storm ground surveys. *Electronic J. Operational Meteor.*, **13**, 32–45.

Bluestein, H. B., J. C. Snyder, and J. B. Houser, 2015: A multiscale overview of the El Reno, Oklahoma, tornadic supercell of 31 May 2013. *Wea. Forecasting.*, **30**, 525–552, doi:10.1175/WAF-D-14-00152.1.

Hyvärinen, O., and E. Saltikoff, 2010: Social media as a source of meteorological observations. *Mon. Wea. Rev.*, **138**, 3175–3184, doi:10.1175/2010MWR3270.1.

Kumjian, M. R., 2013: Principles and applications of dual-polarization weather radar. Part I: Description of the polarimetric radar variables. *J. Operational Meteor.*, **1 (19)**, 226–242, doi:10.15191/nwajom.2013.0119.

Picca, J., and A. Ryzhkov, 2012: A dual-wavelength polarimetric analysis of the 16 May 2010 Oklahoma City extreme hailstorm. *Mon. Wea. Rev.*, **140**, 1385–1403, doi:10.1175/MWR-D-11-00112.1.

Romine, G. S., D. W. Burgess, and R. B. Wilhelmson, 2008: A dual-polarization-radar-based assessment of the 8 May 2003 Oklahoma City area tornadic supercell. *Mon. Wea. Rev.*, **136**, 2849–2870, doi: 10.1175/2008MWR2330.1.

Seimon, A., J. T. Allen, T. Seimon, E. Edwards, S. Talbot, and D. Hoadley, 2014: The El Reno Survey Project: Crowd-sourced database development, synchronous photogrammetric observations and 3-D mapping of the largest documented tornado. *Proc. 27th Conf. on Severe Local Storms*, Madison, WI, Amer. Meteor. Soc., 13.5, [Available online at https://ams.confex.com/ams/27SLS/webprogram/Paper254094.html.].

Smyth, T. J., T. M. Blackman, and A. J. Illingworth, 1999: Observations of oblate hail using dual polarization radar and implications for hail-detection schemes. *Quart. J. Roy. Meteor. Soc.*, **125**, 993–1016, doi: 10.1002/qj.49712555512.

Witt, A., 2014: High-resolution phased array radar observations of an Oklahoma hailstorm producing extremely-large hail. *Proc. 27th Conf. on Severe Local Storms*, Madison, WI, Amer. Meteor. Soc., 165, [Available online at https://ams.confex.com/ams/27SLS/webprogram/Paper253994.html.].

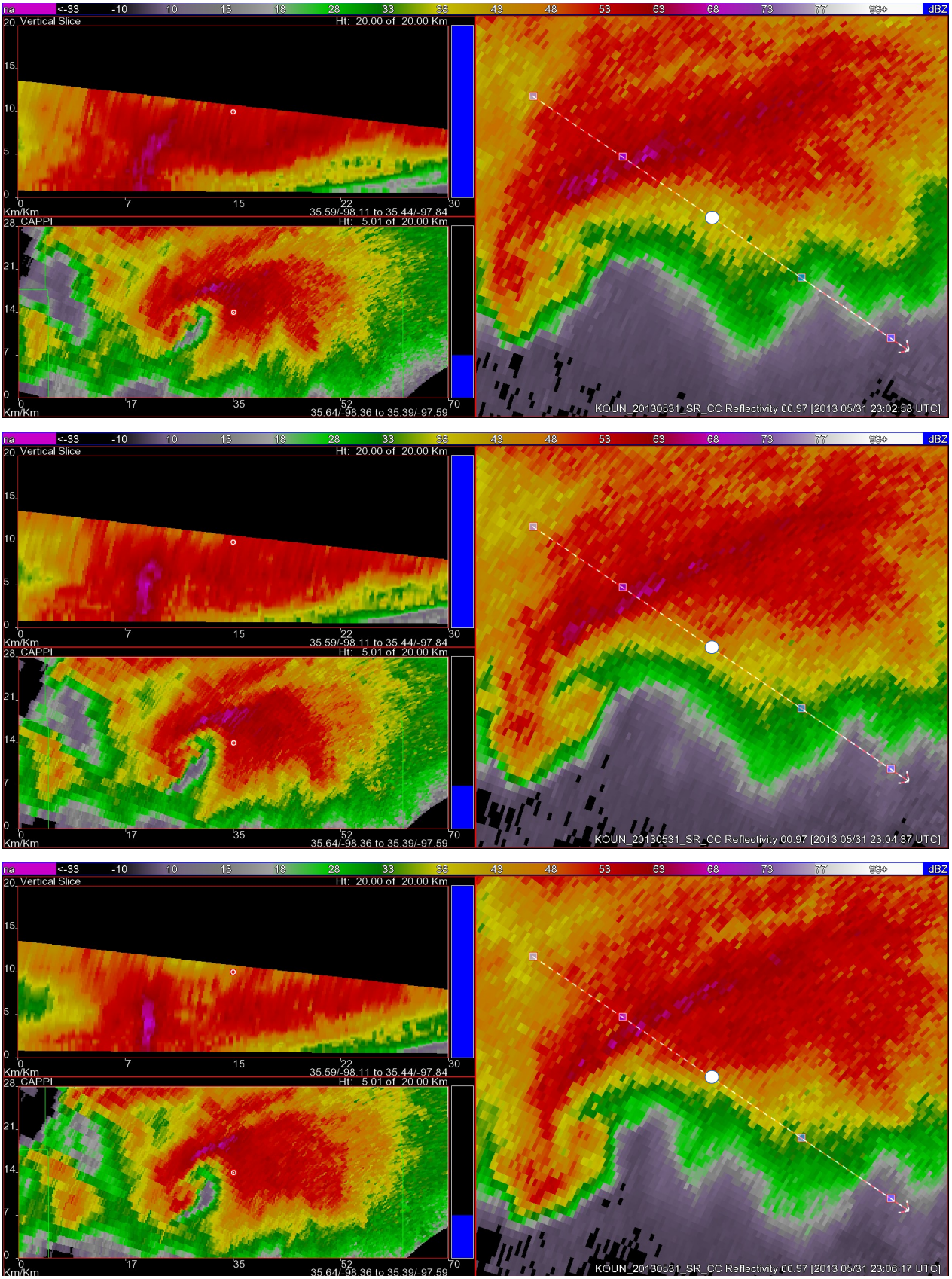

FIG. 4. Reflectivity at 2302:58 UTC (top), 2304:37 UTC (middle) and 2306:17 UTC (bottom). For each image, the upper-left panel is the vertical cross section along the dashed line shown on right-side panel of the 0.97° elevation scan, and the lower-left panel is the horizontal cross section at the 5 km ARL height. The white circle on right-side panel shows the location of the FFH.

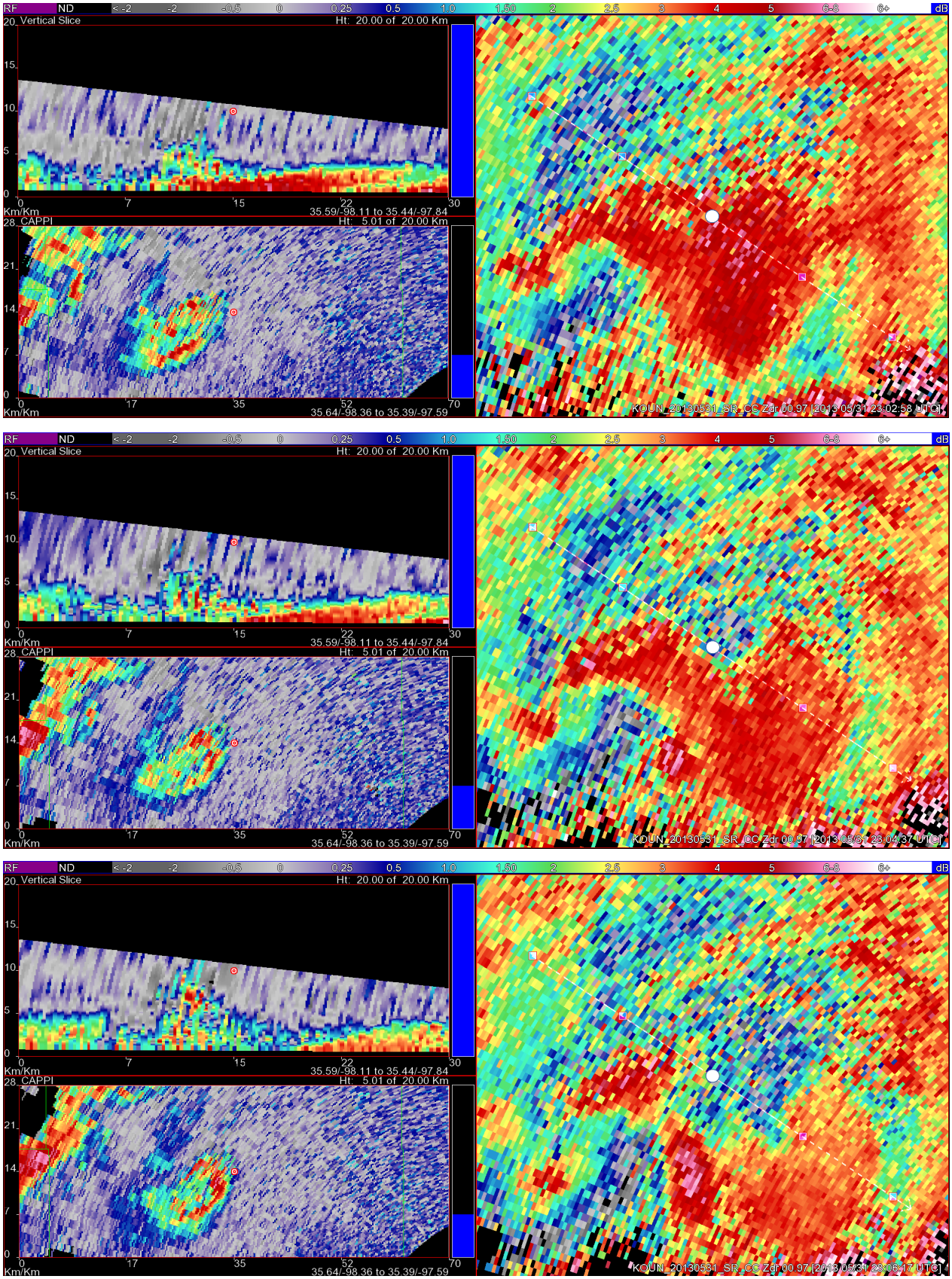

FIG. 5. Same as Fig. 4, except for differential reflectivity.

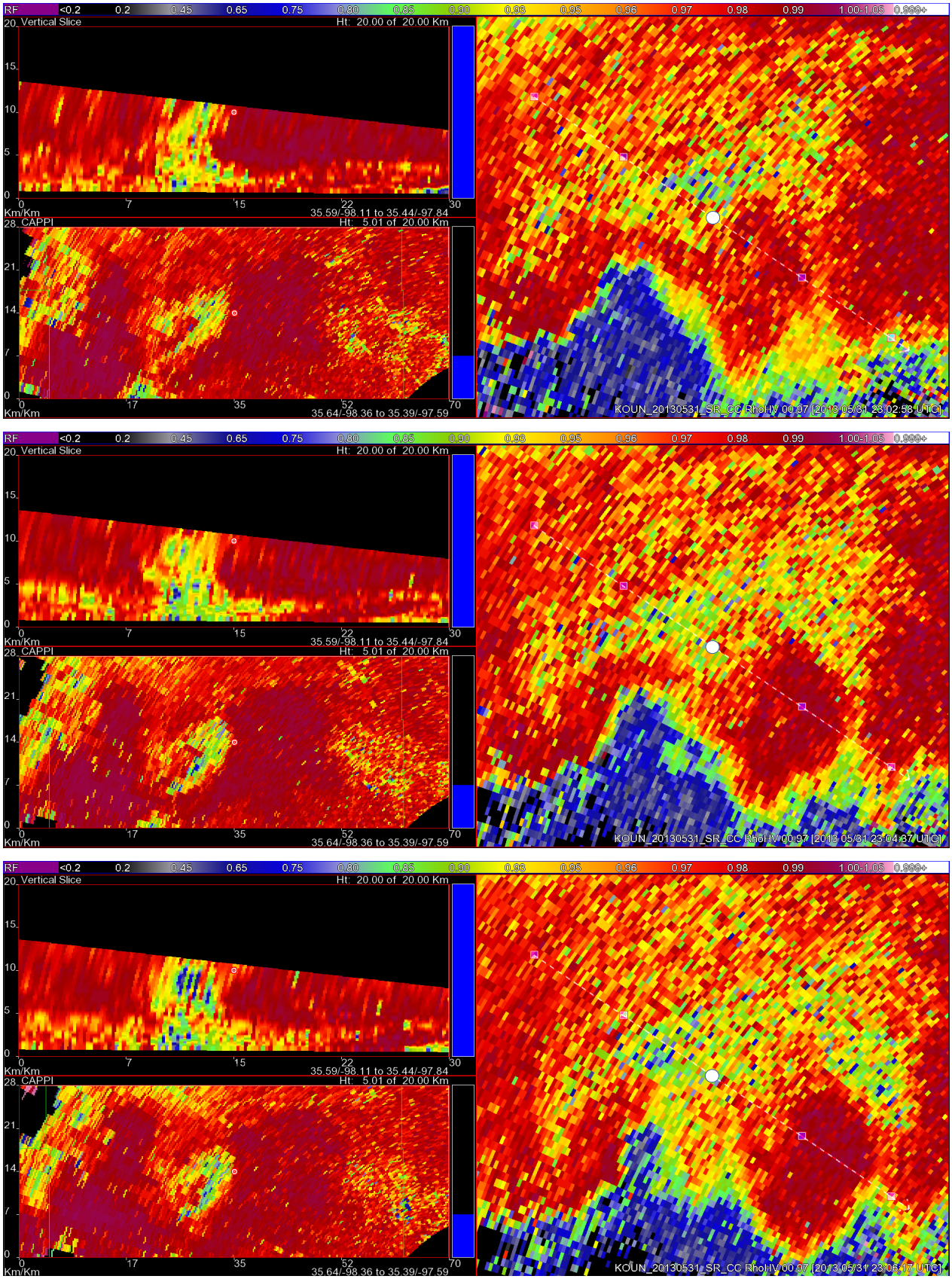

FIG. 6. Same as Fig. 4, except for co-polar correlation coefficient.

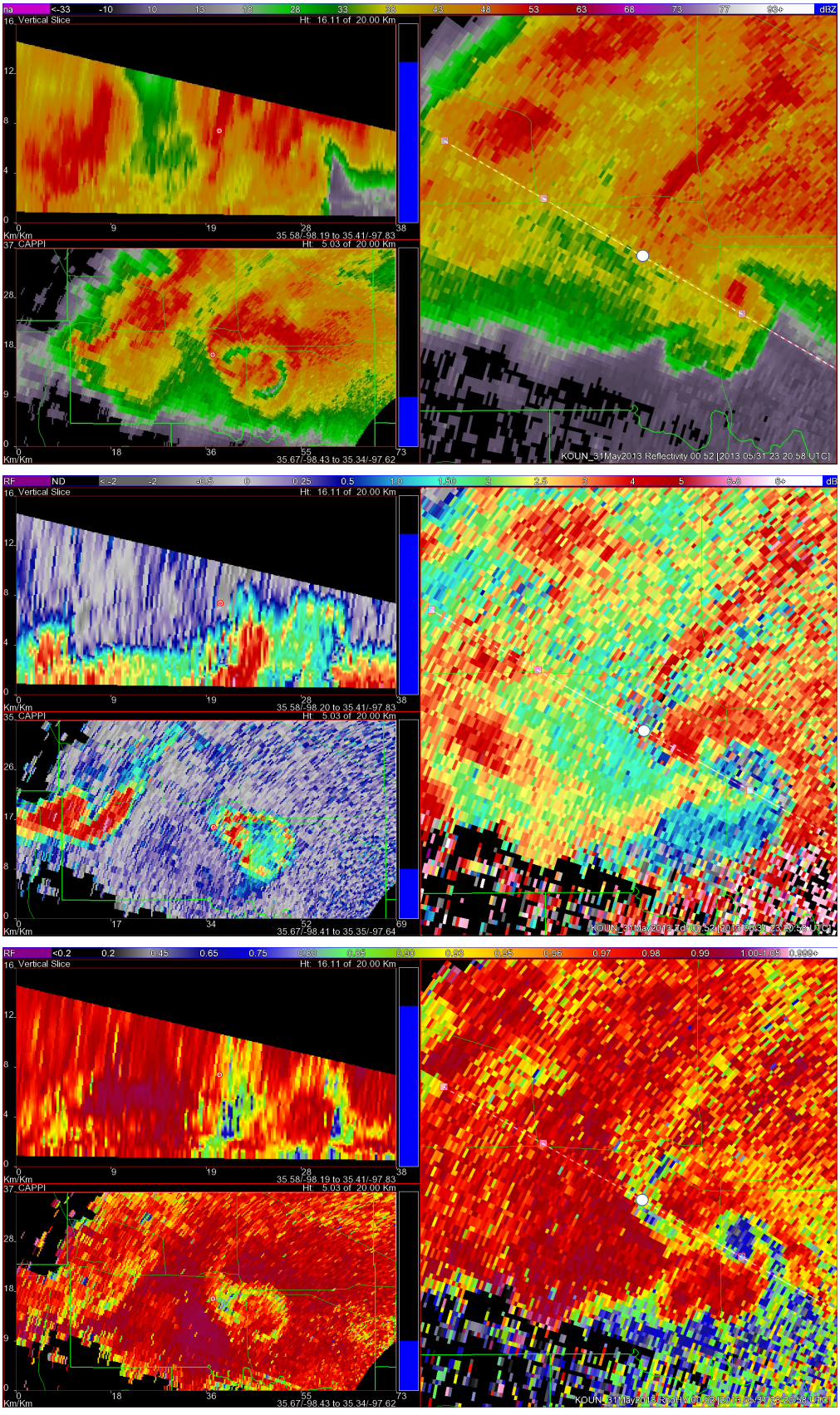

FIG. 7. Reflectivity (top), differential reflectivity (middle), and co-polar correlation coefficient (bottom) at 2320:58 UTC. For each image, the upper-left panel is the vertical cross section along the dashed line shown on right-side panel of the 0.52° elevation scan, and the lower-left panel is the horizontal cross section at the 5 km ARL height. The white circle on right-side panel shows the location of the HEH.

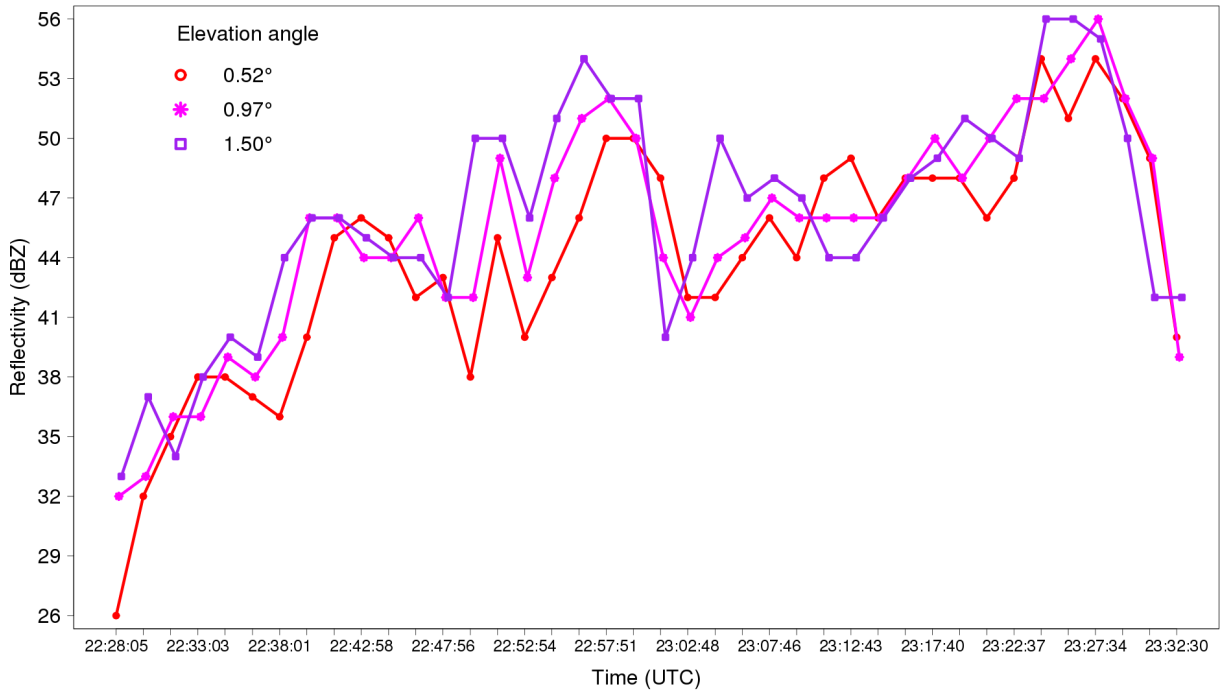

FIG. 8. Time series of LA-*Z* above the FFH location.

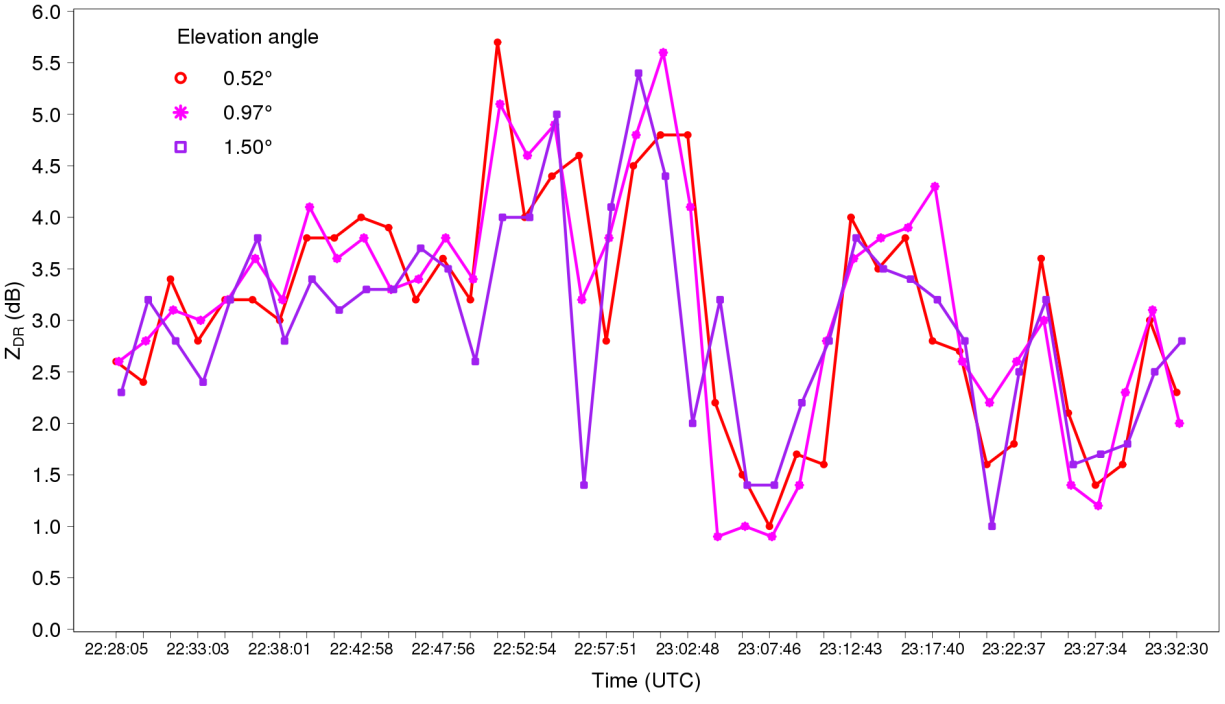

FIG. 9. Time series of LA-Z_{DR} above the FFH location.

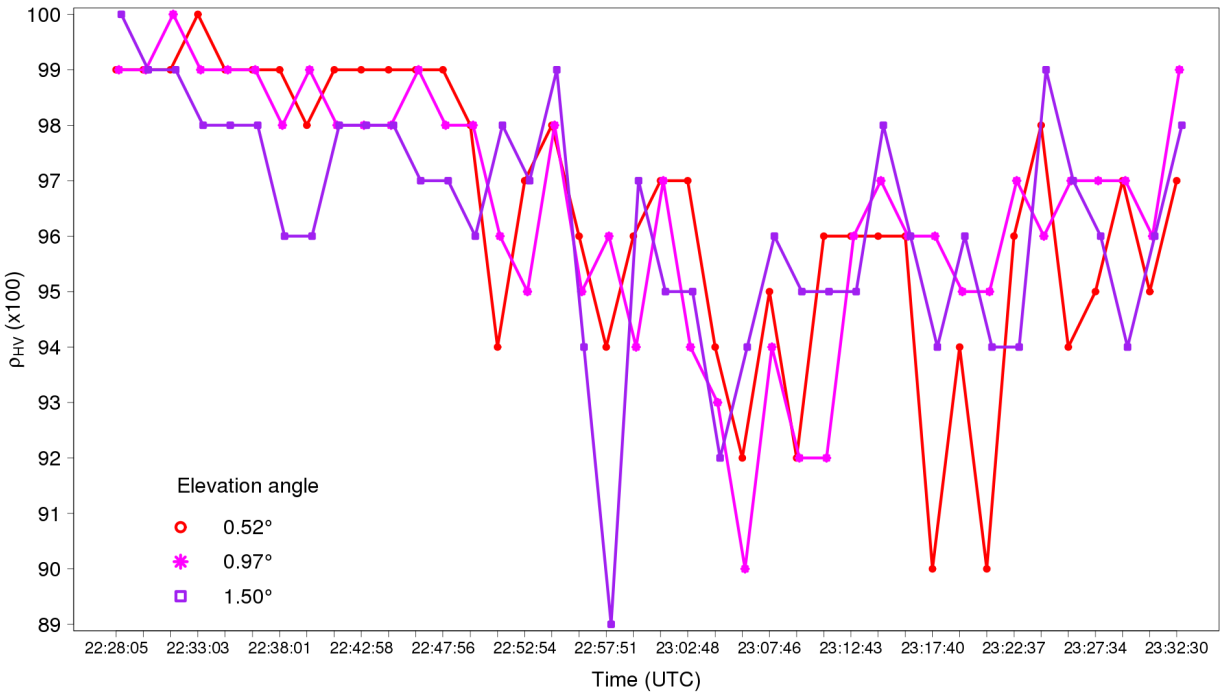

FIG. 10. Time series of LA-ρ_{HV} above the FFH location.

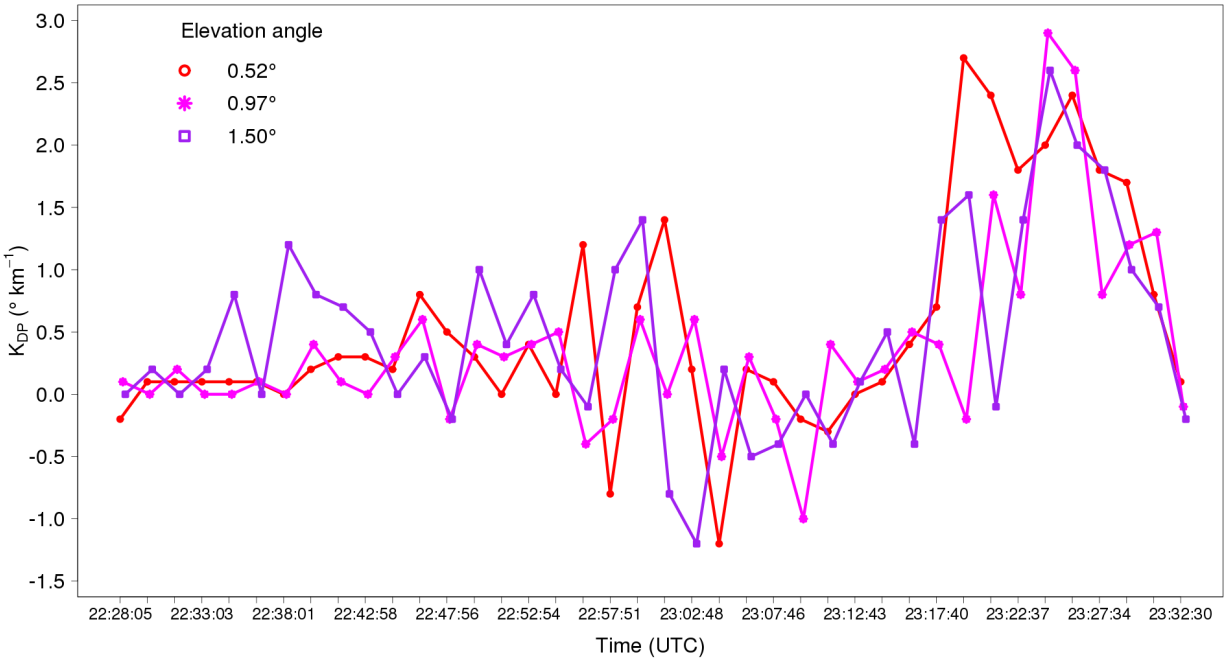

FIG. 11. Time series of LA-K_{DP} above the FFH location.

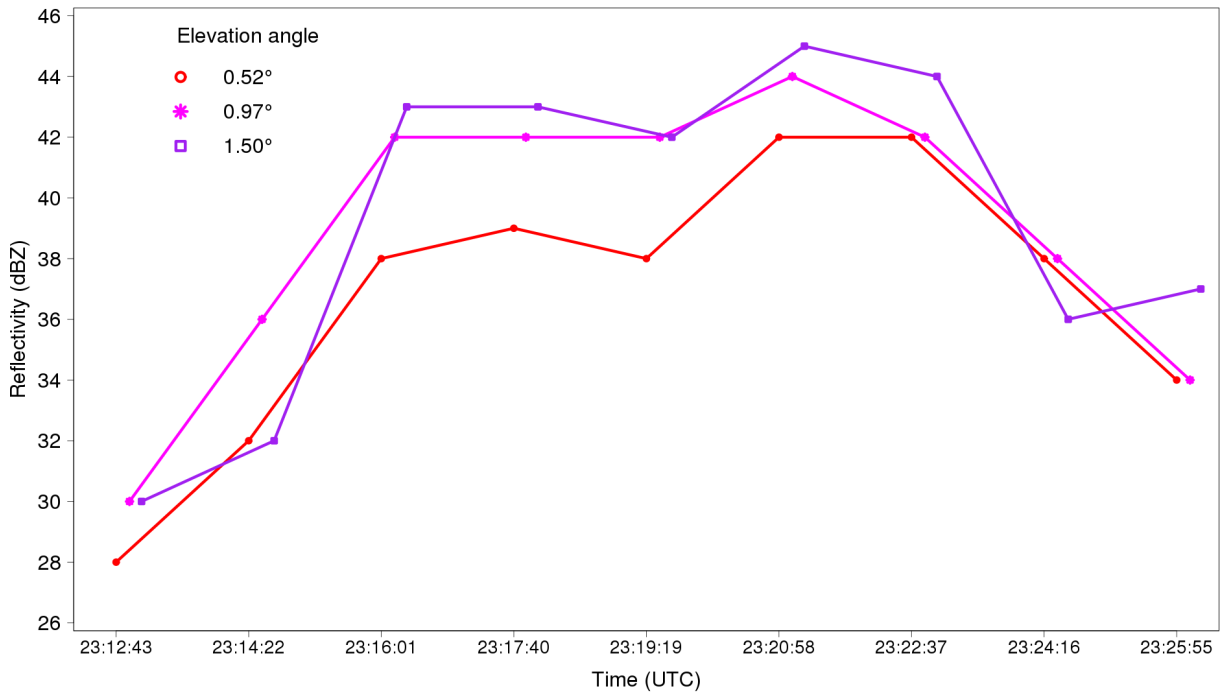

FIG. 12. Time series of LA-Z above the HEH location.

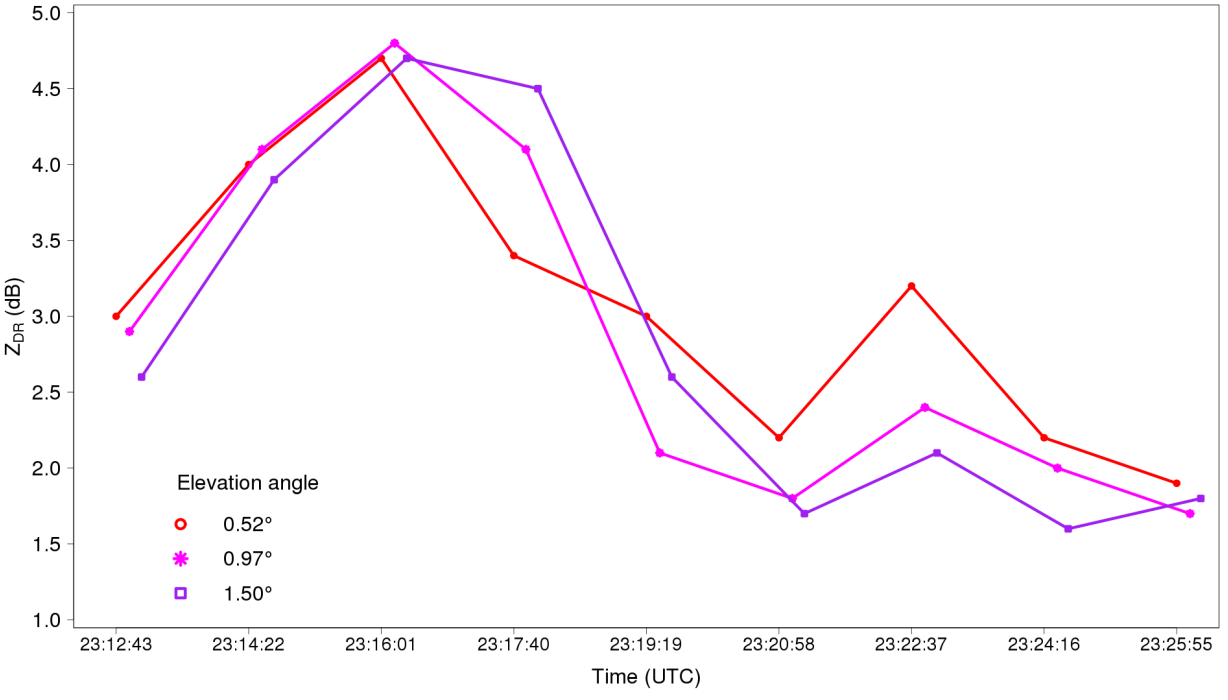

FIG. 13. Time series of LA-Z_{DR} above the HEH location.

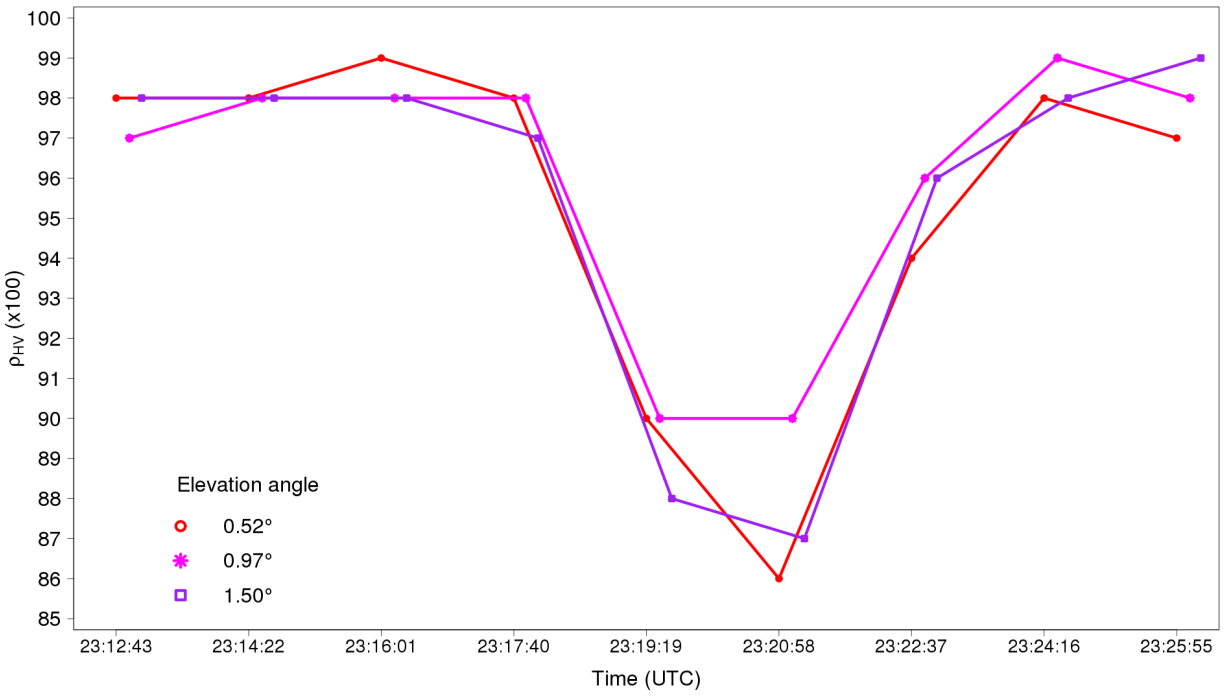

FIG. 14. Time series of LA-ρ_{HV} above the HEH location.

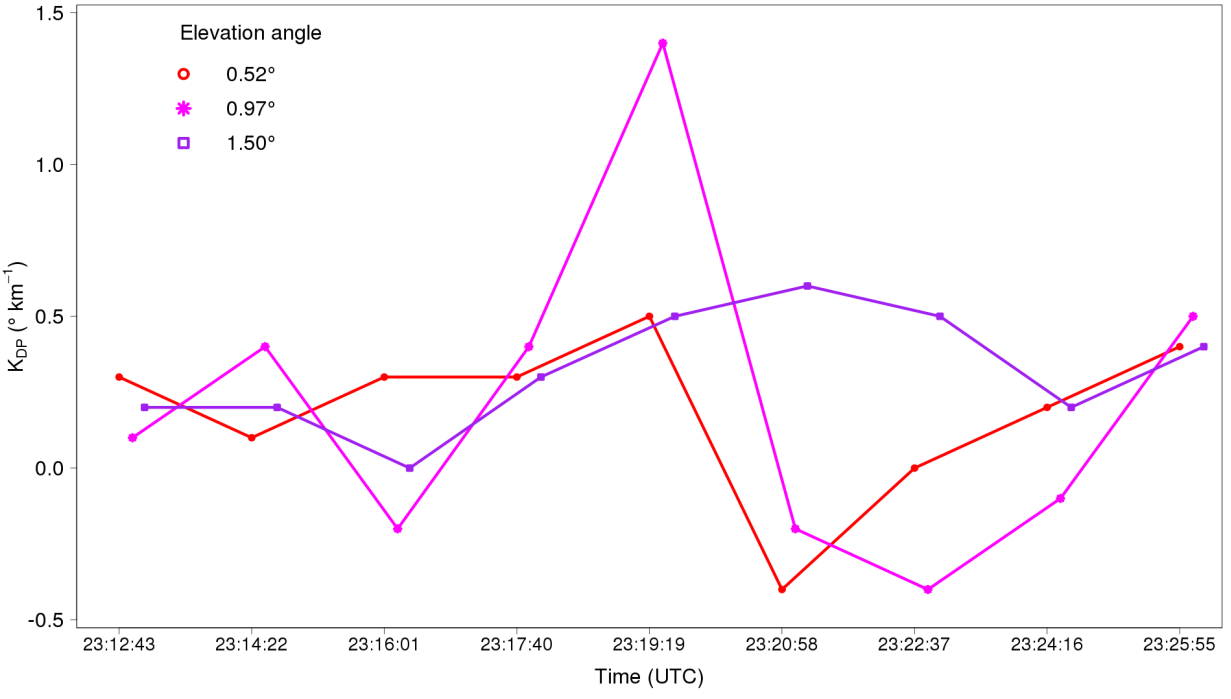

FIG. 15. Time series of LA-K_{DP} above the HEH location.